In situ observations of microphysics, electric fields, and lightning in the trailing stratiform region of a mesoscale convective system

Andrew G Detwiler[1] and Patrick Kennedy[2]

[1]South Dakota School of Mines and Technology
[2]Colorado State University

November 22, 2022

Abstract

We use airborne observations to extend a previous analysis by Lang and Rutledge (2008) of remotely sensed radar and lightning mapping array observations of the 11 June 2000 asymmetric mesoscale convective system (MCS) that moved through the primary observation region of the Severe Thunderstorm Electrification/Precipitation Study in northeastern Colorado and northwestern Kansas. We analyze in detail aircraft observations, radar, and remotely-mapped lightning discharges from a portion of the MCS that was starting to produce a bow echo during the time of the aircraft mission. The observations are interpreted to indicate the presence of a rearward and downward-sloping positive charge layer detraining from a mature cell in the leading convective region. In the convective cell the positive charge region was at an altitude of 10 km MSL. It then descended and crossed the 6 km MSL altitude plane 40 km to the rear of the leading convective region. A pattern of rearward and downward propagating lightning discharges from the upper convective region to trailing stratiform region was associated with this layer. The pattern persisted over a period of at least 8 minutes within which time 3 major lightning discharges initiated in the convective region and propagated rearward into the trailing stratiform region through the positive charge layer. Lightning initiation was not observed in the trailing stratiform region during the hour the aircraft was sampling it. The lack of lightning initiation in the trailing stratiform region is attributed to relatively weak electric fields there.

Posted on 22 Nov 2022 — The copyright holder is the author/funder. All rights reserved. No reuse without permission. — https://doi.org/10.1002/essoar.10502660.1 — This a preprint and has not been peer reviewed. Data may be preliminary.

In situ Observations of Microphysics, Electric Fields, and Lightning in the Trailing Stratiform Region of a Mesoscale Convective System

Andrew Detwiler [1] **and** Patrick Kennedy [2]

[1]Atmospheric and Environmental Sciences Program and Department of Physics, South Dakota School of Mines and Technology, Rapid City, SD 57701.

[2]Atmospheric Sciences Department, Colorado State University, Ft. Collins, CO 80523

Corresponding author: Andrew Detwiler (Andrew.Detwiler@sdsmt.edu)

Key Points:

- Aircraft microphysical and electrical observations are obtained during two passes through a developing mesoscale convective system at the -10°C level.
- A positive charge layer is identified in the trailing stratiform region near this level
- Lightning discharges in the stratiform region initiate in the convective region and propagate outward into the stratiform region in association with this charge layer.
- The charge layer extends beyond the maximum extent of the lighning

Abstract

We use *in situ* airborne observations to extend a previous analysis by Lang and Rutledge (2008) of remotely sensed radar and lightning mapping array observations of the 11 June 2000 asymmetric mesoscale convective system (MCS) that moved through the primary observation region of the Severe Thunderstorm Electrification/Precipitation Study in northeastern Colorado and northwestern Kansas. We analyze in detail *in situ* aircraft observations, radar, and remotely-mapped lightning discharges from a portion of the MCS that was starting to produce a bow echo during the time of the aircraft mission. The observations are interpreted to indicate the presence of a rearward and downward-sloping positive charge layer detraining from a mature cell in the leading convective region. In the convective cell the positive charge region was at an altitude of 10 km MSL. It then descended and crossed the 6 km MSL altitude plane 40 km to the rear of the leading convective region. A pattern of rearward and downward propagating lightning discharges from the upper convective region to trailing stratiform region was associated with this layer. The pattern persisted over a period of at least 8 minutes within which time 3 major lightning discharges initiated in the convective region and propagated rearward into the trailing stratiform region through the positive charge layer. Lightning initiation was not observed in the trailing stratiform region during the hour the aircraft was sampling it. The lack of lightning initiation in the trailing stratiform region is attributed to relatively weak electric fields there.

1 Introduction

In this work we address the question of how charge is organized in mesoscale convective systems (MCSs)and how lightning initiates and propagates through relatively quiescent anvils and stratiform regions adjacent to thunderstorm convective regions associated with strong vertical motions. These non-convective regions are regions through which commercial aircraft often pass as they divert around the convective cores to avoid icing, larger graupel and hail, frequent lightning, and turbulence. In these non-convective regions lightning may occasionally initiate and propagate in-cloud or from cloud-to-ground, but often most of the lightning that is observed in these regions initiates in the more highly electrified convective region and propagates outward into the more-weakly electrified anvils and stratiform regions. (e.g. Lang et al. 2004b). Lightning from these stratiform regions may present a hazard to passing aircraft, or outdoor activities on the ground beneath, even though the active convection is 10's of kilometers away. In addition, aircraft and rockets passing through such stratiform regions, even when infrequent or no lightning is occurring there, have been observed to trigger lightning which has caused damage to the passing vehicle. This indicates there can be significant charge present in these regions even in the absence of observed lightning. A classic example of unintentional rocket-triggered lightning is the rocket-triggered lightning event that occurred during the launch of the Apollo 12 mission to the moon from Kennedy Space Center on November 14, 1969. A better understanding of storm electrical processes in these regions and the behavior of lightning in them will lead to better assessments of hazards associated with aircraft and rockets flying through them, and hazards of conducting outdoor activities on the ground beneath them.

The charge distribution within MCS stratiform regions has been extensively studied using balloon-borne electric field meters. See Stolzenburg et al. (1998). A schematic depiction of charge structure in a trailing stratiform region behind leading convective line derived from their work is shown in Figure 1. The schematic is also adapted in light of discussion and figures presented in Lang and Rutledge (2008) specifically applicable to the case discussed in this work. Charged hydrometeors detrain from the convective region and trail behind as the leading convective region propagates to the right in the figure. These detrained regions typically contain charged hydrometeors of both signs, with different signs dominating in different layers to produce different net charges in the vertically-stacked layers extending out into the stratiform region.

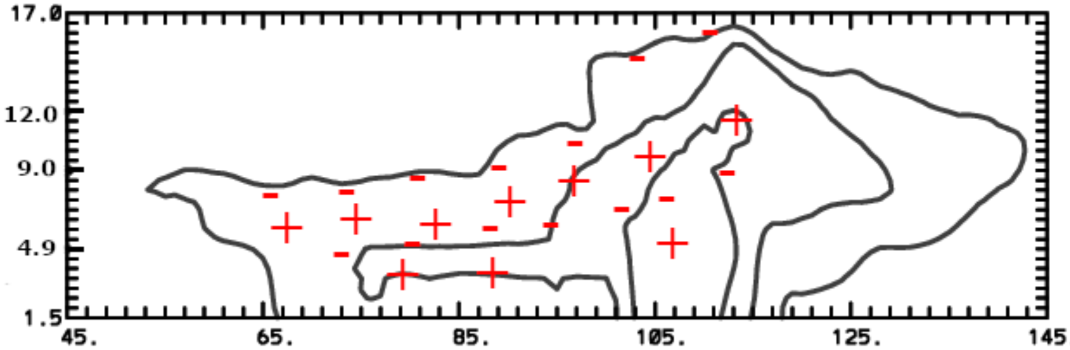

Figure 1: The diagram represents a vertical cross-section of an MCS moving to the right, which is eastward in the actual case presented below. Black contours are radar reflectivity starting at 15 dBZ and increasing by increments of 10 dBZ to 45 dBZ. Axes are distance in kilometers east of an arbitrary origin. Red +/- symbols delineate layers of charge with sign alternating in the vertical. A normal vertical tripole consisting of upper positive, middle negative and lower positive charge regions is depicted in the convective region where the reflectivity contours bulge upward and there are strong vertical winds. Horizontally extensive regions of charged hydrometeors detrained from the convective regions are carried rearward by the storm-relative winds and descend. A relatively thin negative screening layer is found at the top of the cloud, and often a thin positive charge layer is associated with the melting level beneath the stratiform region.

The regions of net charge spread horizontally into sheets tilting downward and rearward due to the gradual descent of the charged hydrometeors as they trail behind the leading convective region. Kuhlman et al (2006) and Calhoun et al. (2012) point out, based on results of numerical storm simulations including electrical processes, that these "regions" may not be continuous but may be broken into flattened ribbon-like or pancake-like volumes intermingled with each other such that in a time-average sense the charge distribution ends up resembling the continuous layers depicted in Figure 1.

Dye and Willett (2007), Dye et al. (2007), and Dye and Bansemer (2019) present observations from horizontal aircraft passes through stratiform anvil regions left behind propagating Florida thunderstorm clusters that also can be interpreted in terms of a layered charge structure like that depicted in Figure 1. They report nearly constant radar reflectivity and vertical electric fields as an instrumented aircraft travels horizontally 10's of kilometers outward away from the convective region through the stratiform region. Constant electric field is consistent with charge distributed in horizontally extensive layers. The microphysical character of the stratiform regions were sampled by the aircraft with a series of horizontal passes at several altitudes. A broad size spectrum of hydrometeors was observed throughout the observed depth of the stratiform region contrary to what might be expected if size sorting is preferentially removing larger hydrometeors from upper regions and causing them to accumulate in lower regions. Dye and Willett (2007) hypothesize that in several of the cases they observed, a weak mesoscale updraft may have maintained supersaturation leading to nucleation of new and further growth of old ice hydrometeors in this trailing region, accounting for the maintenance of a broad spectrum of hydrometeor sizes over a range of altitudes. Mesoscale upward motion may have been sufficient to maintain liquid water saturation in some regions leading to the presence of liquid droplets that cause riming growth on ice hydrometeors and continued non-inductive charge separation. (See also Rutledge et al. 1993.) Dye and Willett (2007) also suggest that, even in the absence of an updraft and supercooled liquid water, a weak non-inductive ice-ice collision mechanism not involving riming may have continued separating charge in the stratiform region. Though weaker than non-inductive charging accompanied by riming, due to it's occurring in a large volume of cloud, they suggest that this collision-based non-inductive charging process may still be strong enough to separate enough charge to maintain significant electric fields in the stratiform regions.

Other aircraft observations of layered charge in stratiform regions trailing behind convective regions have been reported. Mo et al. (2003) report horizontally extensive uniform vertical electric fields observed by two aircraft in coordinated flight along tracks perpendicular to the storm motion direction at two altitudes in an Oklahoma squall line system. The observed fluctuating airborne electric field observations were interpreted as being due to the aircraft passing through relatively thin horizontal charge regions extending rearward behind the advancing convective line. These observations will be discussed in more detail in the discussion section below.

We present here additional aircraft observations combined with radar and lightning mapping array observations in the trailing stratiform region of a High Plains MCS. The lightning mapping array utilized in this study is more sensitive than the one utilized in the work of Dye, Willett, Bansemer and colleagues cited above, yielding better-resolved lightning observations. Also, the High Plains MCS we study has a more organized circulation pattern than the Florida storms. Comparison between these studies provides new insights into electrification and lightning in stratiform precipitation and anvil regions associated with convection.

2 Background

There are several mechanisms by which charge can be separated and rearranged within stratiform regions. If charge of one sign is preferentially on larger hydrometeors, and the opposite charge is preferentially on smaller hydrometeors, gravitation will continue to separate charge. Such charging also can be the result non-inductive charge separation resulting from collisions between ice hydrometeors, one of which is riming. (e.g. Takahashi, 1978) Such collisions can occur in stratiform regions in which there are weak embedded vertical motions (e.g. Detwiler and Heymsfield, 1987), or perhaps larger regions of mesoscale uplift. (Dye and Willett, 2007; Dye et al. 2007; Dye and Bansemer, 2019) that are sufficient to maintain supersaturation with respect to liquid water in mixed-phase regions. Even when vertical motions are too weak to maintain supersaturation, leading to the absence of liquid water, non-inductive collisional charge separation can occur during hydrometeor collisions, albeit more weakly than when riming is occurring (Luque et al. 2016). In addition, when vertical electric fields are present, inductive charge exchange during collisions is possible. Finally, lightning propagating through the region can deposit and rearrange charge.

In the absence of *in situ* charge separation in the stratiform region, charge density in the plumes detrained from the convective region will be modified with time. It will decrease with distance due to turbulent dispersion in the spreading horizontal region containing the detrained charged hydrometeors. Recombination between small ions and oppositely charged hydrometeors will reduce the net charge on hydrometeors. In the absence of new particle nucleation, or breakup of existing particles following collisions (Phillips et al. 2017), the number concentration of hydrometeors in the stratiform region is expected to decrease with distance behind the convective region as the layer spreads horizontally due to turbulent dispersion and aggregation. The physical thickness of the layers also will increase due to turbulent dispersion and size sorting of hydrometeors.

The persistence of organized charge layers for several 10's of kilometers or more rearward from the convective region argues that the processes leading to charge density decrease are relatively slow, and/or that continued charge separation by one or more of the mechanisms discussed above is countering charge dissipation processes.

In the Mo et al. 2003 study cited above two aircraft were flying vertically stacked in a direction perpendicular to the storm motion and well behind the leading convective line. Observations from the lower aircraft near the 0 ºC level showed abrupt sign reversals of the vertical component of the vector electric field **E** (E_z), consistent with the aircraft flying horizontally along relatively thin horizontally-extensive charge regions with occasional undulations of the regions or slight variations in aircraft altitude leading to the aircraft transitioning from above to below the thin charge region or vice-versa. There was no distinct microphysical signature associated with these sheets of charge. These results were interpreted to indicate that the charge layers were relatively thin (100's of meters) and horizontally extensive (10's of km) in the direction perpendicular to storm motion.

Observations from the upper aircraft near the -10 ºC showed smaller variations in E_z while crossing the stratiform region behind and parallel to the leading convective line. The E_z component was always positive polarity but ranged from 10 to 25 kV m^{-1}, with the locations of the minima and maxima in fixed locations relative to the storm radar structure. These observations can be interpreted as the aircraft being above a positive charge layer or below a negative one with charge density slowly varying horizontally by up to a factor 2x. Microphysical observations were not available from the upper aircraft.

Shepherd *et al.* (1996) presented several examples of thin positive charge layers associated with the melting level in trailing stratiform regions as mapped using electrical balloon soundings. They discussed several mechanisms that might maintain such layers near the melting level. Many of these mechanisms involved the phase-change of water there, such as breakup of melting snow aggregates. No *in situ* mechanisms have been suggested that may lead to the maintenance of thin layers of charge in stratiform layers at higher colder cloud levels, as in the case of the upper aircraft in the Mo et al. (2003) study.

Relatively thin regions of charge in stratiform regions have also developed in numerically simulated storms when electrical processes are included in the model. Numerical simulations of two different large supercellular storms are described in Kulman et al. (2006) and Calhoun et al. (2014). The numerical model used included parameterizations of charge separation, and lightning initiation and propagation. The simulated storms generated relatively extensive horizontal charge layers in their more stratiform downshear regions. Neither of these storms had stratiform regions extending more than approximately 30 km from the convective region, which is a relatively small distance compared to those observed in many squall-line and other MCS storms. These layers in the simulated storms also were not as extensive as those investigated in Florida thunderstorm complexes by Dye and Willett (2007), Dye et al. (2007), and Dye and Bansemer (2019). In these two simulated cases diagnostics showed negligible charge separation occurring outside of the convective region. One infers that these downshear horizontal layers are the result of advection of charged hydrometers outward from the convective regions of the simulated storms with vertical shearing of the horizontal wind stretching the advected charge into horizontally extensive layers and turbulent mixing leading to more thermodynamic stability. The stability acts to damp vertical motion, with stability and damping increasing with distance from the convective region (Detwiler and Heymsfield 1987). Stretching and turbulence may break these layers into discrete pancake-like regions or patches that in time-averaged sense resemble continuous regions.

Kulman et al. (2006) tested several different non-inductive charge separation parameterizations in an ensemble of simulations of the first thunderstorm mentioned above. Some of these produce more extensive layers than others. Non-inductive charge separation without riming is not included in any of these parameterizations, so there can be no non-inductive separation in liquid-water-free portions of the stratiform regions in these simulations. Calhoun et al. (2014), in their simulation of the second storm mentioned above, note that their simulation in this case did not produce lightning initiations in the more distant reaches of the downshear stratiform region, although such lightning initiation was observed in the actual storm on which the simulation is based. These results are consistent with the possibility that the model did not adequately represent the microphysical evolution of the stratiform region, or that a mechanism for continued charge separation in the absence of supercooled cloud water might be needed in storm electrification models to reproduce observed lightning initiation in these regions.

Lang and Rutledge (2008) (hereafter LR) analyzed lightning and radar observations of a large asymmetric MCS that moved through the observation area of the Severe Thunderstorm Electrification/Precipitation Study (STEPS) (Lang et al. 2004a) in northeast Colorado and western Kansas on the afternoon and evening of June 11 2000. This was a complex storm and LR focus on several different features in different regions of interest in different phases of development of this large MCS that evolved over 5 hours of observations. They analyze reflectivity structures and lightning activity and look at relationships between bulk reflectivity and lightning flash rate statistics during these periods. Of particular interest to the present study, they note that 99% of VHF lightning sources detected by the STEPS lightning mapping array (LMA) in this storm in the portion of the storm discussed below occurred within 10 km of the leading convective line. Lightning in the trailing stratiform regions was infrequent, and almost always initiated in the convective line and propagated rearward. They note two typical propagation paths for this rearward-propagating lightning. There was an upper path leaving the convective region at about 9 km MSL and descending as it propagated rearward. A second typical path left the convective region at about 6 km MSL and propagated rearward at constant altitude. Based on the observed behavior of lightning discharges, these “well-travelled” lightning propagation paths can be inferred to be almost always within layers of non-zero net charge (e.g. Williams et al. 1985, Thomas et al. 2004, Coleman et al. 2003, Coleman et al. 2008). The more concentrated the charge, the more branching there will be of the lightning discharges propagating through them (Williams et al. 1985)

One of the periods and regions of focus in the LR study they call the “high wind” event. Straight-line winds associated with a bow-echo radar reflectivity feature developed at the north end of the leading convective region of the organizing storm during the second hour of its development. The storm was taking on the organization of an asymmetric MCS at this time. The South Dakota School of Mines and Technology (SDSMT) armored T-28 research aircraft made a long pass at altitude 6 km MSL (-10 ^{o}C) northwestward through the leading convective line to the rear edge of the trailing stratiform region more than 50 km behind the leading line, reversed course, and passed back through the storm and out the leading edge. The aircraft observations over a period of 40 min coincided with the organization of an initially disorganized collection of convective cells into an organized MCS. Utilizing aircraft kinematic, microphysical, and electric field observations, we explore the microphysical and electrical characteristics of the trailing stratiform region during this time, with particular emphasis on evidence for layers or discrete regions of charge in the trailing stratiform region, and the microphysical and electrical characteristics associated with these charged regions.

3 Observations

The storm that is the subject of this study occurred on June 11, 2000 during STEPS. The armored research aircraft made microphysical and electrical observations within the storm. Of particular relevance to this study the aircraft carried three optical array probes for hydrometeor observations. These included a Particle Measuring Systems (PMS), Inc., 2D-cloud probe, a Stratton Park Engineering Corporation (SPEC) high-volume precipitation spectrometer (HVPS-2) probe, and a SDSMT custom-built hail spectrometer optical array probe. Using these 3 probes, hydrometeors with diameters between 50 μm and 5 cm were observed. The aircraft also was equipped with a Droplet Measurement Technologies (DMT) cloud liquid water probe and a suite of six New Mexico Institute of Mining and Technology (NMIMT) Model 100 electric field meters, two total temperature probes, and a pitot-static total pressure sensor for deriving true airspeed. Vertical winds were computed by inverting the aircraft equation of motion (Kopp, 1985).

Other observing systems used in this study include the Colorado State University CHILL (CSU-CHILL) and National Center for Atmospheric Research (NCAR) Spol S-band polarimetric Doppler radars, the NMIMT LMA which provided 3-dimensional maps of lightning channels, and the National Lightning Detection Network which provided locations and characteristics of cloud-to-ground lightning events. (See Lang et al. 2004a for more description of STEPS observing systems.)

LR describe the early history of this MCS as an area of multicellular convection that developed in southern Colorado and propagated eastward while being advected northeastward by mid-tropospheric flow, moving towards northwest Kansas. This convection was detected by the STEPS radar network by 19:00 UTC. The leading edge of a group of convective cells that had begun to organize into a linear system came within 100 km of the westernmost STEPS radar, the CSU-CHILL radar, by 21:00 UTC. At 21:30 UTC the armored aircraft began its mission to observe the interior of the storm at the -10ºC level (roughly 6 km MSL). It entered the leading edge of the storm then flew northwestward through the leading convective region and out into the trailing stratiform region. During the period of airborne observations this area of convection organized into a leading convective line with a trailing stratiform region growing behind it as the leading line propagated eastward. Weak southwesterly steering flow continued to advect the whole system toward the northeast. Near 22:00 UTC, as the aircraft reversed course to fly from the rear of the storm back through and out the leading edge, an asymmetric MCS structure developed with strong convection and an eastward bowing radar echo on its northern end where the aircraft was flying. The leading convective line extended off to the southwest from the region of bowing. Severe surface winds were associated with this northern bowing region, and large hail was later produced in several cells on the southern end of the line.

Figure 2 illustrates using radar observations how the northern end of the storm organized between 21:30 UTC and 22:40 UTC, roughly from the beginning to just after the end of the T-28 mission. Figure 2a shows the convective cells as they began organizing. The newest group of cells just inside the 100 km range ring is apparently forming on the leading edge of the outflow from earlier cells to the northwest. Figure 2b shows that the storm evolved from a disorganized cluster of convective cells to a well-organized convective line during this period.

Figure 3 shows the aircraft track overlain on a 6 km CAPPI of the storm, based on CSU-CHILL radar observations at the midpoint time of the mission. The aircraft was in the storm from 21:40 – 22:20 UTC. During the first half of this period it was flying from the leading convective line northwestward into the trailing stratiform region. Near 21:56 UTC it approached the northwestern edge of the stratiform region, made a 180º turn to the right and flew southeastward back through the trailing stratiform region and then out through the leading convective region.

Figure 4 shows vertical cross-sections of (top panel) reflectivity and (bottom panel) ground-relative Doppler velocity along a vertical plane aligned with the red line in Figure 3. Rear-to-front outflow at the leading edge at low levels is triggering new cell development at its leading edge. There is motion in the rearward direction aloft as hydrometeors move from the upper part of the convective region into the trailing stratiform region.

Figure 5 displays the dominant hydrometeor type in this cross-section as determined from S-band polarimetric radar signatures using a fuzzy-logic hydrometeor identification scheme. The hydrometeor identification logic applied here follows the procedures reported in Dolan and Rutledge (2009) and Dolan et al (2013) for X and C-Band radar wavelengths, here adapted for use at S-band wavelengths. The convective region is dominated by graupel, some of which is reaching the ground. Rain is the dominant hydrometeor in the trailing stratiform region below the melting level. Ice crystals dominate the trailing stratiform region from the melting layer up to 8 to 9 km. Above 9 km there is snow and vertical ice.

Figure 6 shows selected *in situ* aircraft observations during the outbound pass at 6 km MSL and until just after the turn to go back through the storm. Included are concentrations of cloud water, small (d < 1 mm) ice particles from the 2D-C probe, large (d > 5mm) particle concentration from the hail spectrometer, temperature, updraft, and vertical component of the electric field. The aircraft encounters non-electrified developing convective cells ahead of the main convective region, beginning around 21:40 UTC (21.66 decimal hours). Peak cloud water concentrations in these cells are less than 1 g m^{-3}, and there are low concentrations of small ice particles. Just after 21:45 UTC (21.75 decimal hours) the aircraft enters the main convective region with updrafts reaching 10 m s^{-1} and cloud water concentrations peaking at around 2 g $m^{-3}$with negligible small ice concentration (the low concentration shown here is almost entirely artifacts due to water collecting on the tips of the 2D-C optical array probe used to monitor small hydrometeors and shedding through its observation volume). After 21:46 UTC (21.77 decimal hours) the aircraft passes from the nearly precipitation-free updraft region into a mixed-phase region with large ice, small ice, and much lower cloud water concentrations.

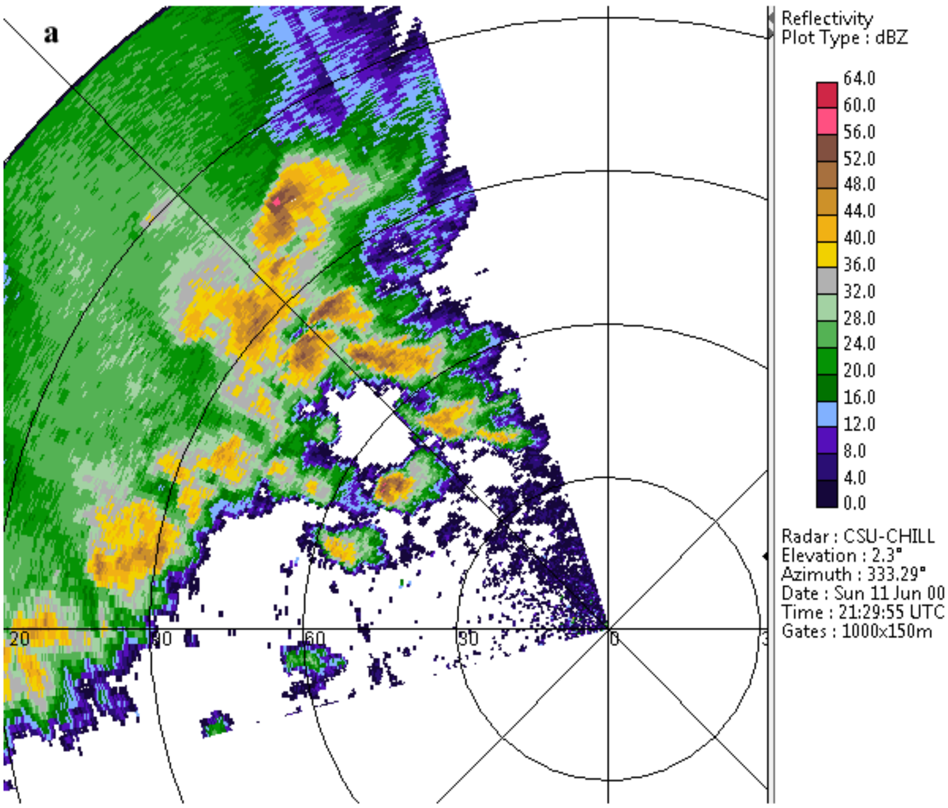

Figure 2a: 2.3^o elevation angle sector PPI from CSU-CHILL radar showing storm beginning to organize in the STEPS region at 21:30 UTC. Radar reflectivity factor color bar is to the right.

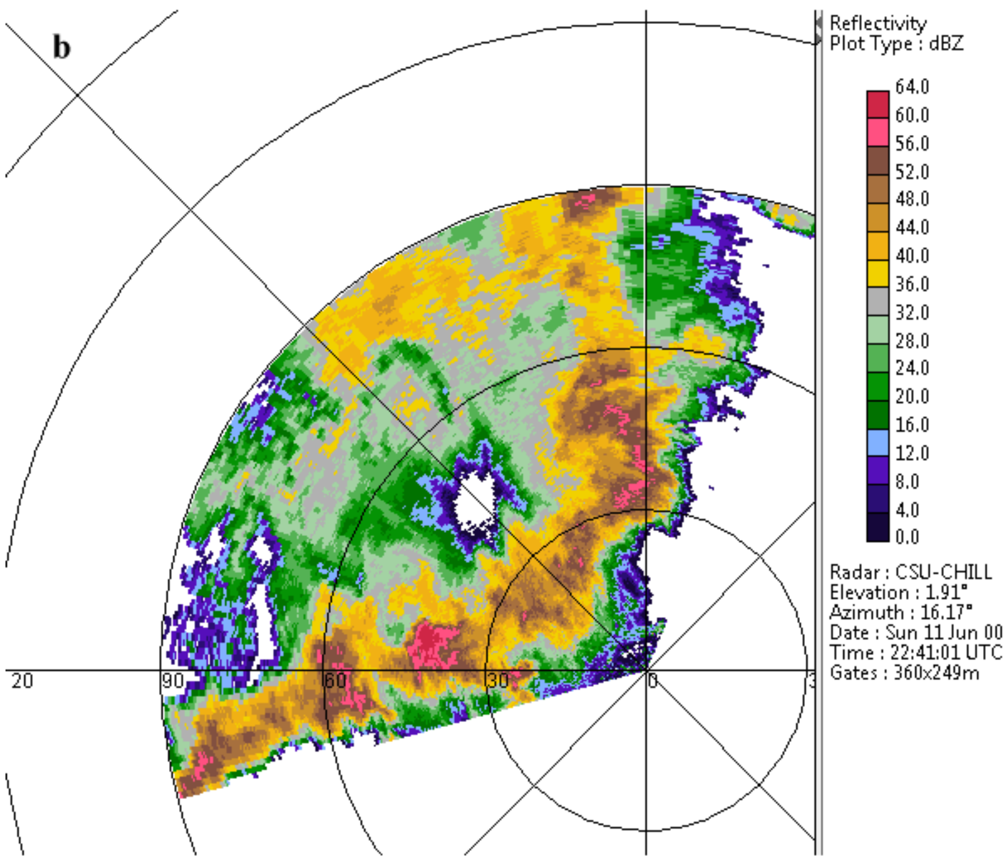

Figure 2b: As in Figure 2a, but 1.9^o PPI sector scan at 22:41 UTC showing a well-organized leading convective line nearing the radar.

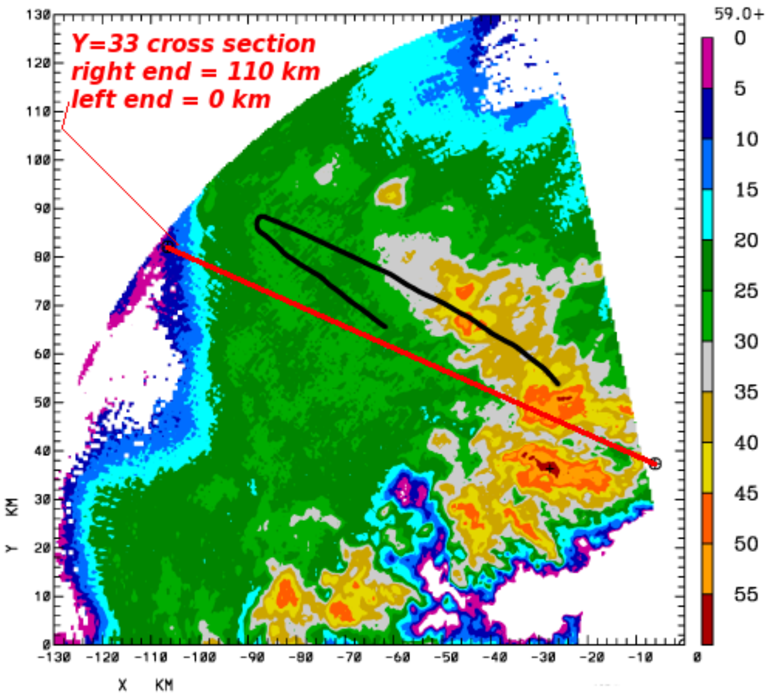

300

301 *Figure 3: CSU-CHILL CAPPI at 6 km at 22:00 UTC showing path of aircraft from 21:50 – 22:21*
302 *UTC relative to radar-observed storm structure at the midpoint time of the mission. Red line*
303 *represents orientation of vertical cross-sections in Figures 4 and 5.*

304

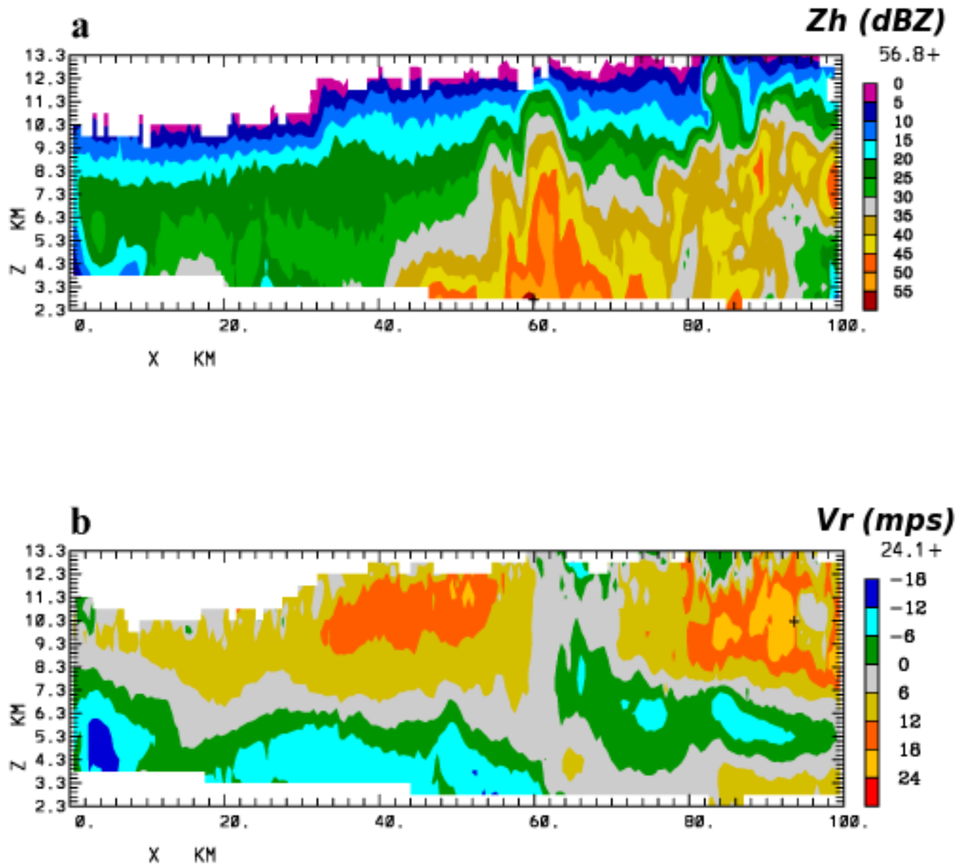

Figure 4: (a) Vertical radar reflectivity cross-section aligned with the red line indicated on Figure 3. (b) Radar Doppler velocities in same cross-sectional plane with positive values corresponding to motion away from the radar (leftward in the figure).

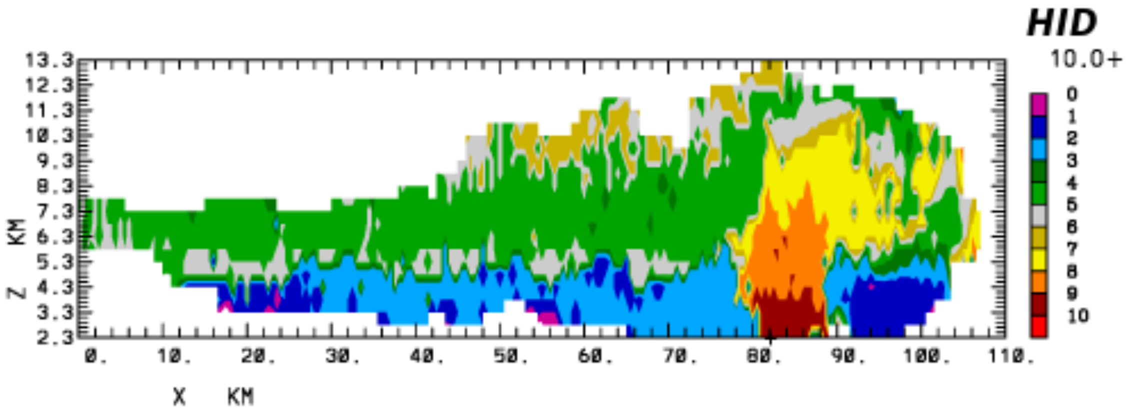

Figure 5: Vertical cross-section showing dominant hydrometeor types corresponding to reflectivity and Doppler velocity structures in Figure 4 along the plane indicated in Figure 3. The color-coding is as follows: 0 – unclassified, 1 – drizzle, 2 – rain, 3 – aggregates/snow, 4 – ice crystals, 5 – wet snow, 6 – vertical ice, 7 – low density graupel, 8- high density graupel, 9 – hail, 10 – big drops.

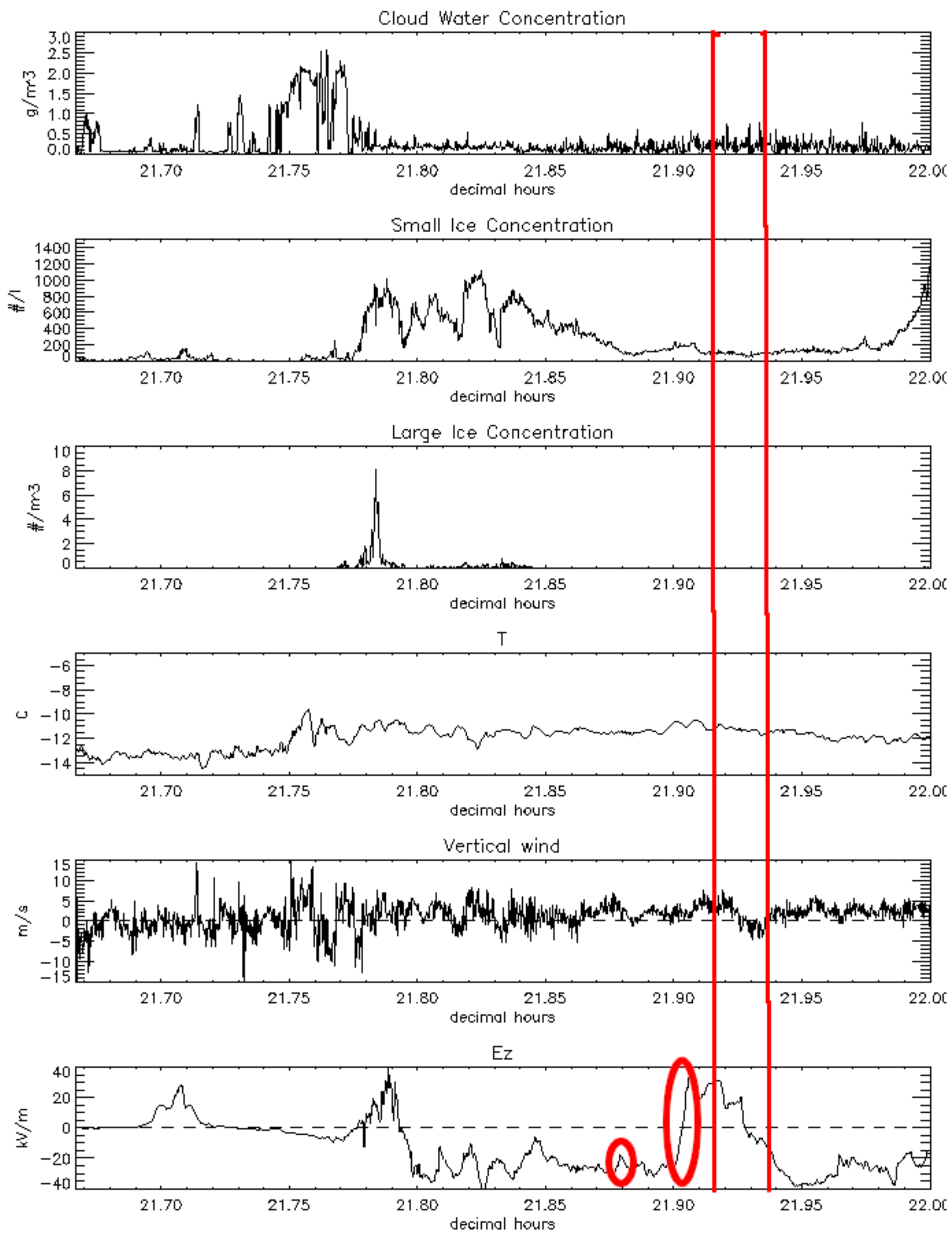

Figure 6: Aircraft observations from 21:40:00 – 22:00:00 (21.66 – 22.00 decimal hours) UTC during outbound pass through storm, showing (upper panel) cloud water concentration, (2nd panel) small ice particle concentration from PMS 2D-C probe, (3rd panel) concentration of particles larger than 5 mm across from hail spectrometer, (4th panel) air temperature, (5th panel) vertical winds, and (6th panel) vertical component of the electric field. Left circled region on lowest panel indicates time of lightning event at 21:52.42 UTC (21.88 decimal hours) reported by pilot and discussed in the text. Right circled region indicates time of rapid flip of E_z from negative to positive at 21:54:00, also discussed in the text. Red vertical lines delineate period over which aircraft did a 180^o reverse course to the right.

The largest hydrometeors are found within the first kilometer (10 sec travel time) into the mixed phase region. Fluctuations in the vertical wind diminish as the aircraft continues into the stratiform region around 21:48 UT (21.80 decimal hours) with initially high concentrations of small ice hydrometeors. These concentrations initially fluctuate but a general decline begins after 21:49 UT (21.82 decimal hours). At 21:55 UT (21.93 decimal hours) the pilot begins his turn, still in-cloud, but noting that he can see the ground from his altitude of 6.1 km MSL, indicating that cloud at and below his altitude was tenuous in this region

We next consider the E_z observations. As the aircraft enters the main convective region at 21:45 UT (21.75 decimal hours) it passes through 3 buoyant updrafts that are nearly precipitation-free at the aircraft level. There is a weak downward directed electric field (negative E_z) in this region, probably due to positive charge overhead. After these updrafts there is a sharp reduction in cloud liquid water as the mixed phase region is entered. Here E_z has a positive 30 kV m^{-1} peak consistent with positive charge below and/or negative charge above the aircraft altitude of 6.1 km MSL (-11^{o}C). By 21:48 (21.80 decimal hours) the aircraft is in the trailing stratiform region with high small ice concentrations, no larger hydrometeors, and negligible cloud water. The vertical electric field component E_z switches to negative and fluctuates between -5 and -40 kV m^{-1}. After 21:52 UT (21.87 decimal hours) E_z settles down to a nearly constant -20 kV m^{-1}. These E_z values are consistent with a widespread horizontal region of positive charge above the aircraft level, or negative charge below.

This most probable interpretation of charge sign is determined by observations at 21:54 UT (21.90 decimal hours) where E_z flips sign from negative to positive over a 25 sec time interval while recovering to nearly the same 20 V m^{-1} magnitude. This abrupt reversal in sign but maintenance of magnitude we interpret as the signature of the aircraft passing through a slightly-sloping horizontally extensive positive charge region that may be associated with an extensive charge region, or collection of charged regions, extending outward and downward from the upper reaches of the convective region and crossing the aircraft altitude at this location. It is less likely that the other possible interpretation of the flip in sign of E_z, a negative charge layer below the aircraft tilting upward through the aircraft altitude, was present. If the hydrometeors mainly originate in the convective region and fall with time, one expects charge regions to be tilting downward and rearward in this region of the storm.

During and after the turn during the period 21:55 – 21:56 UTC, the sign of E_z changes from positive back to negative. See Figures 6 and 7. This change occurs in multiple steps and is not as abrupt as the earlier shift from negative to positive. This suggests the vertical structure of the positive charge was different (less organized) in the region where the aircraft turned compared to conditions in the region of the E_z reversal when the aircraft was outbound before the turn. Figure 3 shows that as the aircraft came out of the turn it was in a region dominated by a different, closer convective cell compared to the region through which it passed on the outbound leg, indicating possibly a different source for hydrometeors in this part of the stratiform region and a less coherent and organized region of positive charge.

Figure 7 shows all three components of **E** for the same period as shown in Figure 6. The components are in a earth-relative coordinate system, where E_z is positive upward, E_y is positive in the horizontal to the north, and E_x is positive in the horizontal to the east. They are computed using the method given in Mo et al. 1999 but with slight modification due to a sixth field meter added to the aircraft instrumentation suite in 2000. The vertical component E_z dominates in the stratiform region observation period shown here. Given the in-cloud environment in which the aircraft is operating the observations have a noise level of +/- a few kV m^{-1}. For the T-28 system the E_x component is the most sensitive to contamination by varying net charge on the aircraft due to hydrometeor impacts, icing, static discharges, etc. The extended period of negative E_z and E_y after the turn is consistent with positive charge above and to the north of the aircraft as it flies southeastward toward an active convective region. (See also Figure 3)

This convective region was producing lightning that in fact had been visually observed by the pilot. While flying outbound through the trailing stratiform region, before passing the location where E_z flipped sign, the pilot reported seeing surrounding cloud illuminated by a lightning event at 21:52:42 UT (21.87 decimal hours). The LMA captured this event as a complex discharge that initiated in the upper portion of this convective region at an altitude near 10 km MSL at that time 10 km east of the aircraft. See Figure 8. Branches of this discharge propagated extensively through the upper storm region. One branch propagated northwestward and sloped downward as it reached 30 km out into the stratiform region. Outer portions of it approached the aircraft altitude but based on LMA observations it was centered in the horizontal around 10 km north of the aircraft at this time. Another branch of the same event went

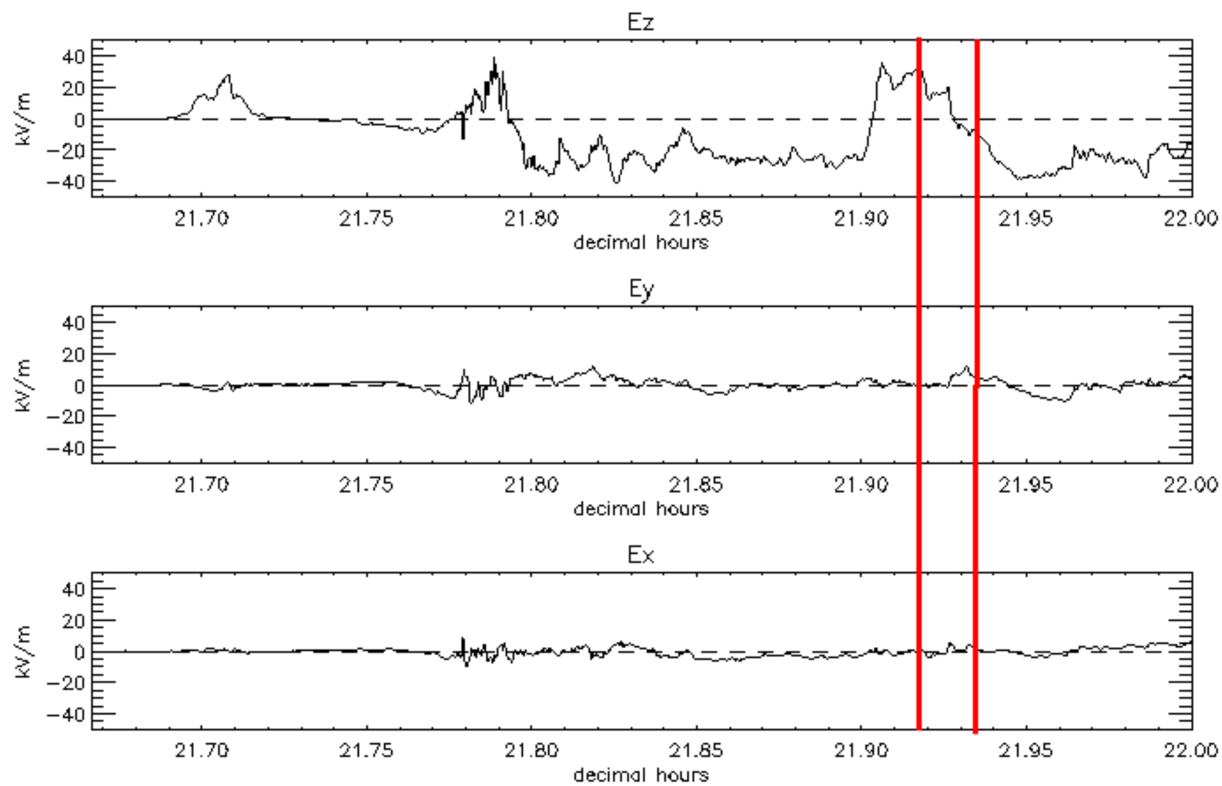

Figure 7: Electric field components E_x(eastward), E_y (northward), and E_z(upward) from storm entry until after the 180^o right reverse course maneuver ending the outbound leg and beginning the inbound leg. The two red lines indicate beginning and ending of turn.

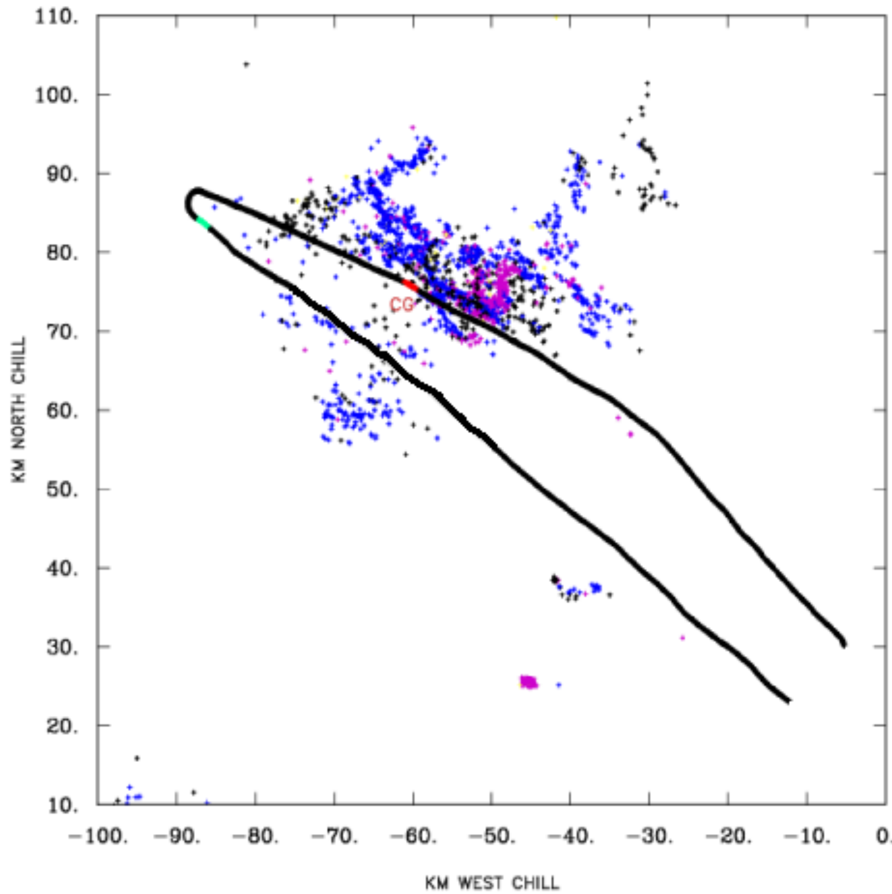

Figure 8: Aircraft track from storm entry at 21:40:00 – 22:20:00 UTC as it flies rearward through the convective then stratiform regions, reverses course to the right, and flies from the rear back out through the leading-edge convective region. LMA VHF source locations shown for complex lightning discharge at 21:52:42 UTC, color-coded by altitude. Purple indicates source altitudes 9-11 km, blue 7-9 km, and black below 7 km. Green track segment indicates location of aircraft-observed rapid reversal of E_z at 21:54:00 UTC. Red track segment indicates location of a radar "skin paint" from the aircraft observed at 22:00:00 UTC.

to ground as a positive cloud-to-ground stroke beneath the convective region. The high density of LMA sources mapped for the rearward propagating branch, considered in light of results reported in LR, suggests this discharge was propagating through a downward sloping positive charge layer originating near 10 km MSL in the convective region and terminating near the 6 km level after covering a horizontal distance of ~40 km.

Over the next 8 min, at least 2 additional lightning events retraced much the same storm-relative path, consistent with a coherent positive charge region extended from the upper convective region rearward and downward into the trailing stratiform region near the aircraft path. This layer or region must have persisted for at least this period of time. This path was one of the two main paths noted by LR for lightning propagating from the convective region into the trailing stratiform region in this region of the MCS. In Figure 9 a projection of LMA source density into a vertical plane aligned along the flight track shows the extensions of LMA sources associated with lightning propagating outward into the trailing stratiform region for the 3 events.

If we characterize this region as a sloping extensive horizontal region of positive charge that has been detrained from the convective region at 10 km MSL and descended to the 6 km MSL level over 40 km of motion relative to the convective region, we can visualize it as in Figure 10 where the angle between the sloping layer and the horizontal aircraft track is estimated as arctan(4/40), or about 6°. If the aircraft takes 22 sec to pass horizontally through the sloping layer then its thickness must be ~300 m. If the magnitude of E_z is taken as 25 kV m^{-1} and this is assumed to be due to a horizontally infinite sheet of charge, the charge per unit area of the sheet is 0.44 (10^{-6}) C m^{-2}. (For an infinite sheet of charge, the perpendicular electric field is independent of distance from the sheet.) If the sheet is 300 m thick, and charge is distributed through it, the volume concentration of charge is 1.5 (10^{-9}) C m^{-3}. Assuming this scenario, this concentration can be taken as characteristic of net charge concentration near the maximum distance lightning is propagating from the convective region outward through this positive layer.

Both the hydrometeor concentrations and the ice water concentration in the stratiform region decreased with distance from the leading-edge convection (Fig. 11). The particle concentration reduction is shown by the general reduction in small particle counts associated with the aircraft course reversal from 21:55 – 21:56 UTC at the outer end of the flight track (Fig. 11 top). Maximum sizes, however, increase in the outer region, consistent with aggregation and size sorting. Estimated ice water concentration also showed a relative minimum in the course reversal area (Fig. 11 bottom panel). The estimated ice water concentration in Figure 11 is based just on particles resolved by the 2D-C probe (peak diameter roughly 2 mm) and so is an underestimate of total ice water concentration. Although some larger particles may not have been included in the observations, there were none larger than 5 mm according to the large OAP probe, the hail spectrometer (See Figure 6.).As shown by the sample hydrometeor images in Figure 12, the general hydrometeor type in the outer stratiform region is rimed snow and aggregates, consistent with the radar-derived hydrometeor type shown in Figure 5.

4 Discussion

Earlier work by LR showed that in the MCS under study, almost all of the lightning in the trailing stratiform region initiated in the convective region and propagated out into the stratiform region, terminating either in-cloud or as a cloud-to-ground discharge. In this study we examine in detail radar, LMA, and airborne *in situ* observations associated with three such lightning events over an 8 min period within one region of the storm as it organized into an asymmetric MCS. Observed electric fields at 6.1 km MSL in the stratiform region, up to a ~25 kV/m, are too small for the initiation of lightning there. Initiation requires fields of the order of 100 kV/m in the mid-troposphere (Griffiths and Phelps1976, Marshall et al.1995, and Marshall et al. 2005). Continued propagation and branching of a discharge initiated near the top of the convective region also will become less likely as distance from its point of initiation increases. Channel resistance lowers the potential of the tip relative to that at the channel origin as the channel extends, such that the potential difference between the channel tip and its environment also decreases. When this potential difference decreases enough, propagation stops. Also, the net charge density in the region through which the lightning propagates very likely diminishes with distance from the initiation region, further hindering propagation. (See Williams et al 1985, and Bazelyan and Raizer 2000.)

We present observations showing that variation of the electric field along the flight track suggests an encounter during the outbound leg of the aircraft with a thin horizontally extensive region of positive charge that detrains from the convective region and descends from ~10 km MSL over the convective region to the aircraft sampling level of 6

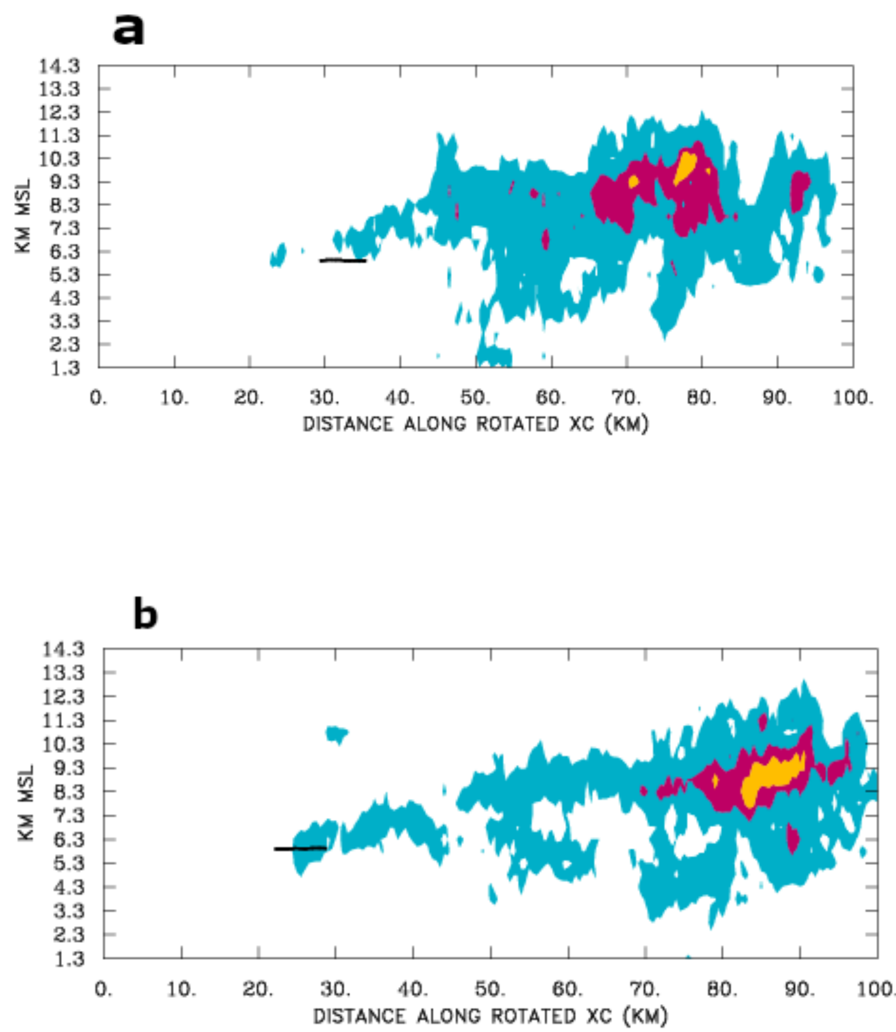
a
KM MSL
14.3
13.3
12.3
11.3
10.3
9.3
8.3
7.3
6.3
5.3
4.3
3.3
2.3
1.3
0. 10. 20. 30. 40. 50. 60. 70. 80. 90. 100.
DISTANCE ALONG ROTATED XC (KM)
b
KM MSL
14.3
13.3
12.3
11.3
10.3
9.3
8.3
7.3
6.3
5.3
4.3
3.3
2.3
1.3
0. 10. 20. 30. 40. 50. 60. 70. 80. 90. 100.
DISTANCE ALONG ROTATED XC (KM)

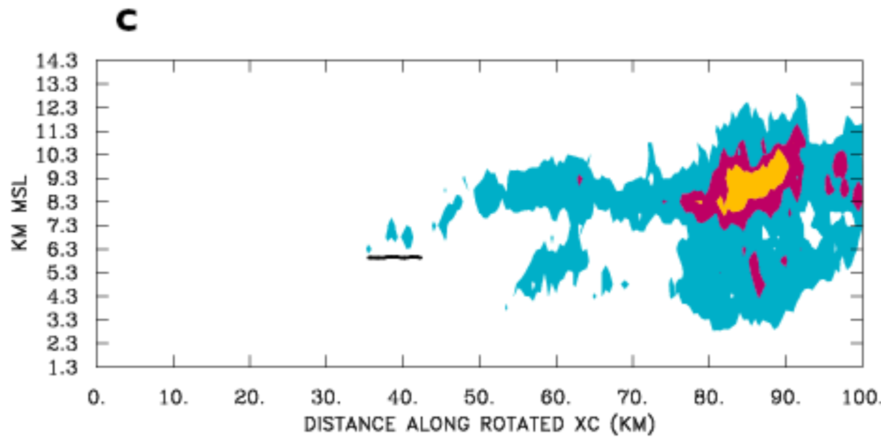

Figure 9: LMA source density projected onto a vertical cross-section aligned with the aircraft track on its return leg through the storm for 3 different one-minute periods containing a lightning event initiating in the convective region (60 – 100 km) and extending out into the stratiform region (30 – 60 km). Panel (a) is 21:52 – 21:53 UTC (aircraft outbound), (b) is 21:57-21:58 UTC (aircraft inbound), and (c) is 21:59 – 22:00 UTC (aircraft inbound). Sources included are within 5 km either side of the vertical plane. Color code for density of sources observed per minute is blue >= 0.8 km^{-3}, red > =4 km^{-3} and yellow >= 24 km^{-3}. Black line indicates aircraft track during the minute projected onto the vertical plane.

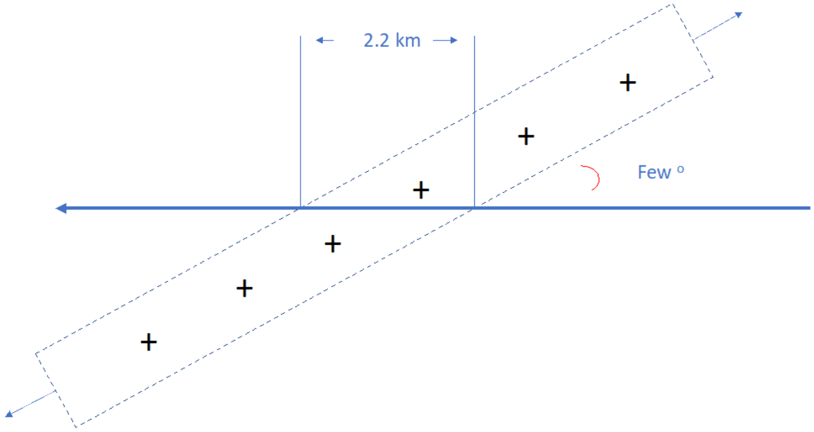

Figure 10: Schematic depiction of aircraft passing horizontally through a sloping charge layer.

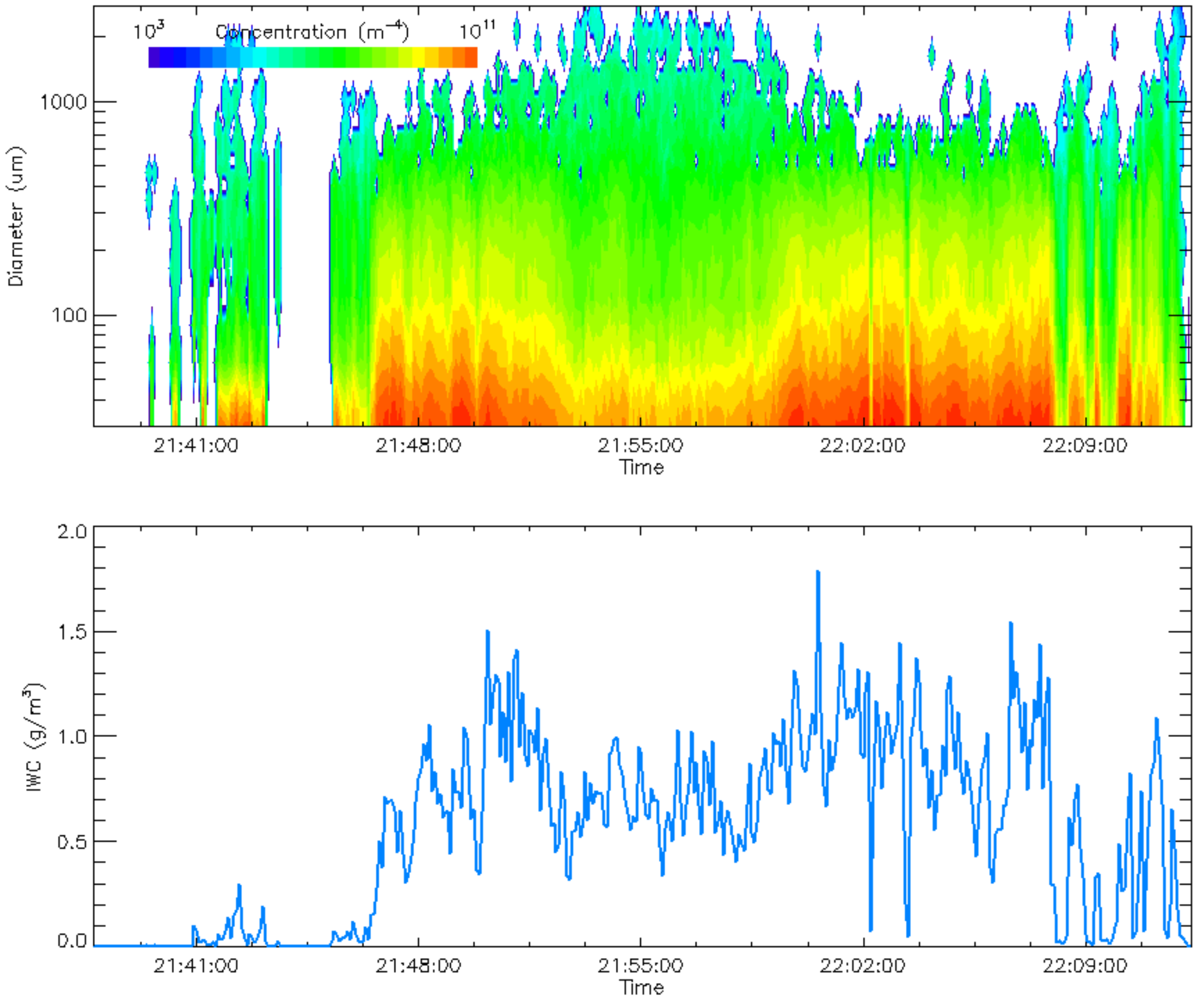

Figure 11: (top panel) color-coded size distribution from the PMS 2D-C probe as a function of time during flight out and back through the storm. The 180^{o} reverse course maneuver occurs from 21:55:00 – 21:56:00. (bottom panel) ice water concentration based on hydrometeors imaged by the 2D-C probe and estimated using a size-mass relationship due to Heymsfield et al. 2010.

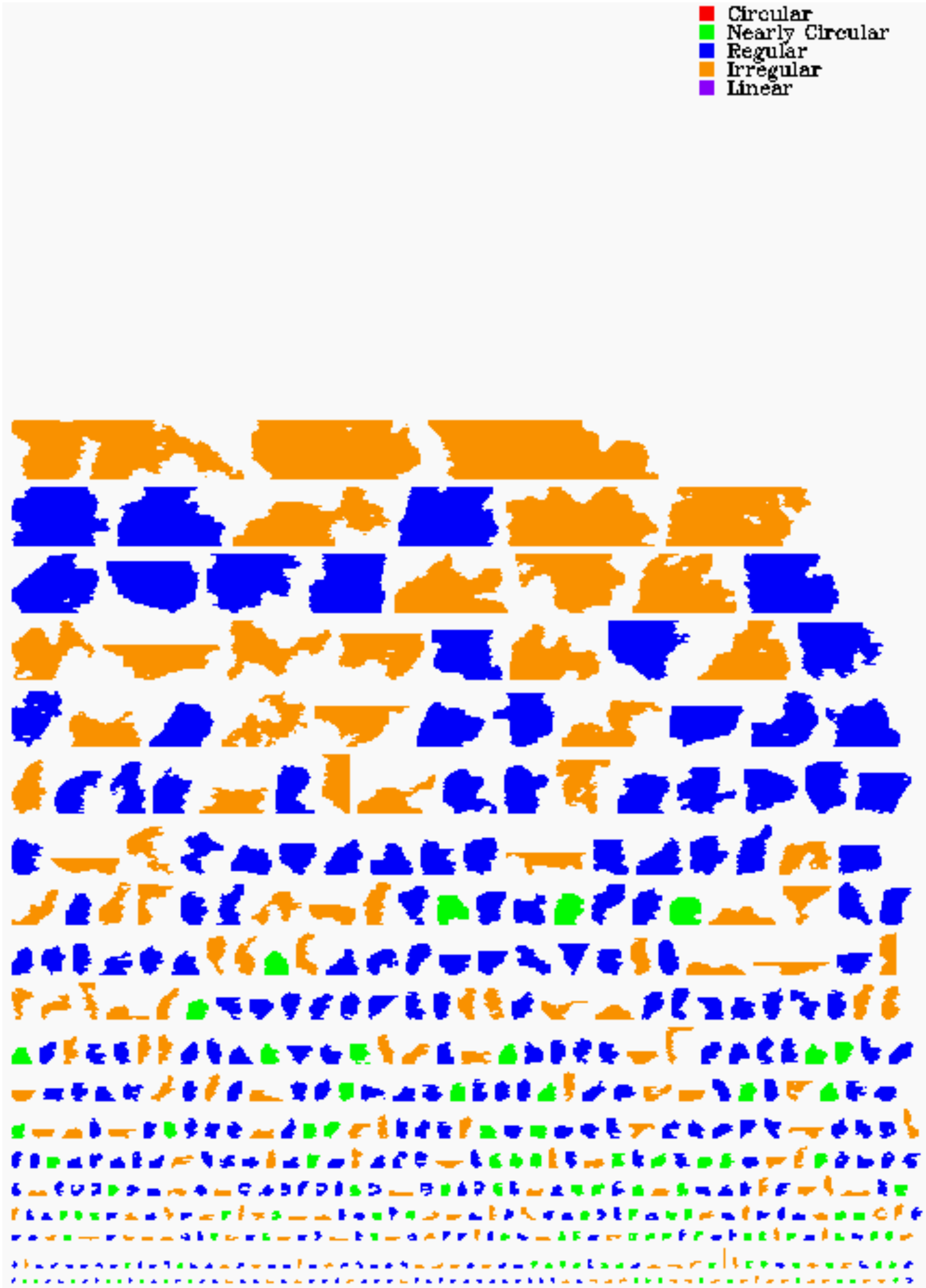

Figure 12: Sample of 2D-C images from the trailing stratiform region acquired between 21:54:06 – 21:54:19, just before the aircraft reversed course to fly back through the storm. The vertical height of the probe sample window is 0.8 mm. For hydrometeors larger than this the upper and/or lower portions are outside the field of view of the probe. Images acquired during this period are ordered from largest to smallest, left to right and top to bottom. The coloring indicates a rudimentary classification into geometric classes ranging from circular to irregular according to the legend at the upper right.

km MSL over a distance of ~40 km. The presence of this upper positive charge region at 10 km MSL in the convective region of the storm was noted by LR based on LMA observations. The observations presented here fit the concept of charge regions developing in convective regions then detraining and forming into sheets or streamers that descend downshear from convective regions. In our case, we infer that the aircraft encountered a positive charge layer at or slightly beyond the furthest extent of lightning propagating from the main convective region based on LMA observations. With some assumptions about the geometry of the charge layer, the charge density in the region of this airborne encounter is estimated to be 1.5 nC m^{-3}.

The projection of LMA source density maps on a vertical plane aligned with the aircraft track show that over a period of 8 minutes three lightning discharges from the upper convective region outward into the trailing stratiform region followed similar vertical trajectories, although paths varied in the horizontal. The first of these was reported by the aircraft pilot based on visual observations while in-cloud and ~10 km from the initiation point. This path persists for 8 minutes or more despite probable alteration of charge distributions due to deposition of charge by continued intracloud and cloud-to-ground lightning, fluctuations in convective motions in the leading convective region, and other microphysical and electrical processes. Coleman et al. (2003) suggest that lightning tends to propagate into electrical potential wells associated with the charge, not along the charge layers themselves. They also show that since the electric field (in this case presumed to be due to a horizontal ribbon or pancake-shaped region of charge) is proportional to the charge density, and the electrical potential is the integration of the electric field, irregularities that develop in the charge density distribution have less effect on the geometry of the potential field than on that of the electric field. Thus the structure of the distribution of potential changes more slowly than that of the distribution of charge. This may facilitate similar lightning trajectories persisting for some period of time despite chaotic storm motions and processes. It was noted that although there was a persisting pattern of lightning propagation in the vertical, in the horizontal the trajectories of the 3 lighting events between 21:52 and 22:00 UT shown in Figure 9 did not coincide so closely (not shown). These 3 discharges passed through cloud volumes separated in the horizontal.

The different character of E_z variation during the outbound transect through the charge layer and the inbound transect (Figure 7) also is consistent with horizontal variability in charge distribution in these detrained charge regions. The character of the positive charge region in this case appear to vary horizontally over distances of less than 5 km. This brings into question using Gauss's law here to quantitatively infer charge density by assuming a horizontally extensive sheet of charge of uniform density in this region of the MCS but the conceptual model should be qualitatively correct.

It should be noted that charge separation leading to relatively thin positive charge regions near the melting level in a trailing stratiform region, as observed by the balloon soundings of Stolzenburg et al. 1998 and by the lower aircraft in the Mo et al. 2003 study, may occur *in situ* at the altitude of the melting layer by one or more microphysically-based mechanisms in addition to advection from the convective region (Shepherd et al. 1996). Relatively thin charge layers higher up, say at the -10 C level, as observed by the upper aircraft in the Mo et al. 2003 study, and as is being presented here, cannot be attributed to any known in situ microphysical mechanism dependent on unique microphysical processes characteristic of that particular temperature level. Advection from convective regions is the most likely mechanism for forming charge layers in stratiform regions at these higher colder levels.

5. Conclusions

This study is based on airborne *in situ* microphysical and electrical observations during two passes through a maturing MCS at the -10° C level along with remotely sensed radar and lightning observations. These observations are limited to one region and a short period within the life-cycle of a large storm. However, they provide insight into processes occurring during the formation and evolution of charge regions in trailing stratiform region associated with such large thunderstorm complexes. The inferences of LR based on remote observations are further supported by combining remote with *in situ* observations. The observations are consistent with downward sloping layers or quasi-organized pancake-like regions of charge detraining from the convective region and advecting out into the stratiform region of an MCS. With some assumptions, charge density in the positive charge region near the rear edge of the stratiform region beyond the region where lightning is propagating is estimated to be 1.5 nC m^{-3} .

In this case there is little evidence for mesoscale upward motion maintaining supersaturated conditions conducive to continued nucleation of new cloud droplets or ice hydrometeors. In the stratiform region the airborne hot-wire liquid water probe records occasional individual ice particle impacts but no continuous signature of cloud liquid water. At greater distances from the convective region smaller hydrometeors are depleted relative to larger ones, consistent with size-sorting and lack of new small hydrometeor formation within the stratiform region. The small end of the hydrometeor size distribution in the stratiform region is not maintained as in the Florida observations of Dye and colleagues. The lack of riming conditions precludes strong non-inductive ice-ice hydrometeor charging within the stratiform region and is consistent with the weakening electric fields at the far reaches of the stratiform region in this case.

It should be recognized that the organization of the MCS described here was evolving during the period of observations; the quasi-steady-state archetypical structure of charge layers with vertically alternating sign of Stolzenburg et al (1998) most likely was not fully developed at this stage of this storm. It is likely that the horizontally patchy character of the E_Z field documented here was related to the multiplicity of still-organizing individual convective sources at the leading edge of the system that contributed to the overall flux of charged hydrometeors into the trailing stratiform region. Additional observations are needed to establish whether the patterns seen in the observations presented here occur generally, or whether they are a coincidence that is unique to this set of observations.

Acknowledgments

Aircraft observations used in this study are archived by the Earth Observing Laboratory (EOL) at the National Center for Atmospheric Research (NCAR) and are described at https://archive.eol.ucar.edu/projects/t28/projects/ . Radar observations from the CSU-CHILL radar are available through http://www.chill.colostate.edu/w/Contacts . Spol radar observations are available from EOL as described at https://data.eol.ucar.edu/dataset/dsproj?STEPS . LMA data are archived at the New Mexico Institute of Mining and Technology (NMIMT)and are described at http://lightning.nmt.edu/nmt_lms/ .The authors thank their many colleagues associated with the SDSMT T-28, CSU-CHILL and NCAR observing facilities, and the LMA group from NMIMT, who contributed to these successful observations in STEPS. We thank Aaron Bansemer for sharing his SODA software for optical array probe data analysis. Timothy Lang provided insightful comments on an early version of this paper. Partial support for this study came from the CSU-CHILL National Radar Facility and the South Dakota School of Mines and Technology

References

Bazelyan, E. M., & Raizer, Y. P. (2000). *Lightning Physics and Lightning Protection*. IOP Publishing, London. 325 pp.

Calhoun, K. M., Mansell, E. R., MacGorman, D. R., & Dowell, D. C. (2014). Numerical simulations of lightning and storm charge of the 29-30 May 2004 Geary, Oklahoma, supercell thunderstorm using EnKF Mobile radar data assimilation. *Monthly Weather Review*, 142, 3977-3997. DOI: 10.1175/MWR-D-13-00403.1

Coleman, L. M., Marshall, T. C., Stolzenburg, M., Hamlin, T., Krehbiel, P. R.,. Rison, W. & Thomas, R. J. (2003). Effects of charge and electrostatic potential on lightning propagation. *Journal of Geophysical Research*, 108(D9), 4298, doi:10.1029/2002JD002718

Coleman, L. M., Stolzenburg, M., Marshall, T. C. & Stanley, M. (2008). Horizontal lightning propagation, preliminary breakdown, and electric potential in New Mexico thunderstorms. *Journal of Geophysical Research*, 113(D9), 4298, doi:10.1029/2007JD009459

Detwiler, A. & Heymsfield A. J. (1987). Air motion characteristics in the anvil of a severe thunderstorm during CCOPE. Journal of Atmospheric Science, 44(15), 1899-1911.

Dolan, B, and Rutledge, S. A. (2009) A theory-based hydrometeor identification algorithm for X-band polarimetric radars. *Journal of Atmospheric and Oceanic Technology* 26(10) 2071-2088.

Dolan, B., Rutledge, S. A., Lim, S., Chandrasekar, V., & Thurai, M. (2013). A robust C-band hydrometeor identification algorithm and application to a long-term polarimetric radar dataset. *Journal of Applied Meteorology and Climatology*, *52*(9), 2162-2186.

Dye, J. E, & Willett, J. C. (2007). Observed enhancement of reflectivity and the electric field in long-lived Florida anvils. Monthly Weather Review, 135, 3362-3380.

Dye. J. E., Bateman, M. G., Christian, H. J.,Defer, E., Grainger, C. A., Hall, W. D., Krider, E. P., Lewis, S. A, Mach, D. M., Merceret, F. J., Willett, J. C., & Willis, P. T. (2007). Electric fields, cloud microphysics, and reflectivity in anvils of Florida thunderstorms. *Journal of Geophysical Research*, 112, D11215. doi:10.1029/2006JD007550.

Dye, J. E., & Bansemer, A. (2019). Electrification in mesoscale updrafts of deep stratiform and anvil clouds in Florida. *Journal of Geophysical Research*: *Atmospheres*,124, 1021-1049. Doi:10.1029/2018JD029130.

Griffiths, R. F. & Phelps, C. T. (1976) The effects of air pressure and water vapour content on the propagation of positive corona streamers, and their implication to lightning initiation. *Quarterly Journal of the Royal Meteorological Society*, 102(432) 419-426. Doi: 10.1002/qj.49710243211

Heymsfield, A. J., Schmitt, C., Bansemer, A., & Twohy, C. H. (2010) Improved representation of ice particle masses based on observations in natural clouds. *Journal of the Atmospheric Science*s, 67, 3303-3318.

Kopp, F. J. (1985). Deduction of vertical motion in the atmosphere from aircraft measurements. *Journal of Atmospheric and Oceanic Technology*, 2(4), 684-688.

Kuhlman, K. M., Ziegler, C. L., Mansell, E. R., MacGorman, D. R. & Straka, J. M. (2006). Numerically simulated electrification and lightning of the 29 June 2000 STEPS supercell storm. *Monthly Weather Review*, 134, 2734-2757.

Lang, T. J., et al., (2004a). The Severe Thunderstorm Electrification and Precipitation Study (STEPS), *Bulletin of the American Meteorological Society*, 85, 1107– 1125.

Lang, T. J., Rutledge, S. A., & Wiens, K. C. (2004b). Origins of positive cloud-to-ground lightning flashes in the stratiform region of a mesoscale convective system. *Geophysical Research Letters*, 31, L10105, doi:10.1029/2004GL019823

Lang, T. J., & Rutledge, S. A. (2008). Kinematic, microphysical and electrical aspects of an asymmetric bow-echo mesoscale convective system observed during STEPS 2000, *Journal of Geophysical Research*, 113, D08213, doi:10.1029/2006JD007709,

Luque, M. Y., Burgesser, R. & Avila, E. (2016). Thunderstorm graupel charging in the absence of supercooled water droplets. *Quarterly Journal of the Royal Meteorological Soc*iety, 142, 2418-2423. Doi:10.1002/qj.2834 .

Marshall, T. C., McCarthy, M.P. & Rust, W. D. (1995). Electric field magnitudes and lightning initiation in thunderstorms. *Journal of Geophysical Research*, 100(D4), 7097-7103

Marshall, T. C., Stolzenburg, M., Maggio, C. R., Coleman, L. M., Krehbiel, P. R., Hamlin, T., Thomas, R. J. & Rison, W. (2005). Observed electric fields associated with lightning initiation. *Geophysical Research Letters*, 32, L03813, doi:1029/2004GL021802

Mo, Q., Feind, R.E., Kopp, F. J. & Detwiler, A. G. (1999). Improved electric field measurements with the T-28 armored research airplane. Journal of Geophysical Research, 104(20), 24485 – 24497.

Mo, Q., Detwiler, A. G., Hallett, J. & Black, R. (2003). Horizontal structure of the electric field in the stratiform region of an Oklahoma mesoscale convective system. *Journal of Geophysical Research*, 108(D7), 4225 doi:10.1029/2001JD001140

Phillips, V. T. J. et al. (2017). Ice multiplication by breakup in ice-ice collisions. Part II: Numerical simulations. *Journal of the Atmospheric Sciences*, 74, 2789-2811 doi: 10.1175/JAS-D-16-0223.1

Rutledge, S., Williams, E., & Petersen, W. A. Lightning and electrical structure of mesoscale convective systems. *Atmospheric Research*, 29(1-2), 27-53.

Shepherd, T.R.,. Rust, W. D. & Marshall, T. C. (1996). Electric fields and charges near 0ºC in stratiform clouds. *Monthly Weather Review*, 124, 919-938.

Stolzenburg, M., Rust, W. D., Smull, B. F. & Marshall, T. C. (1998). Electrical structure in thunderstorm convective regions 1. Mesoscale convective systems. *Journal of Geophysical Research*, 103 (D12), 14059-14078.

Takahashi, T. (1978). Riming electrification as a charge generation mechanism in thunderstorms. *Journal of the Atmospheric Sciences*, 35, 1536-1548.

Thomas, R. J., Krehbiel, P. R., Rison, W., Hunyady, S. J., Winn, W. P., Hamlin, T. &. Harlin, J. (2004). Accuracy of the Lightning Mapping Array. *Journal of Geophysical Research*, 109, D14207, doi: 10.1029/2004JD004549

Williams, E. R., Cooke, C. M., & Wright, K. A., (1985). Electrical discharge propagation in and around space charge clouds. *Journal of Geophysical Research*, 90, 6059-6070.